JOURNAL OF MODERN OPTICS, 2003, VOL. 50, NO. 1, 63–81

Mode degeneracies and the Petermann excess-noise factor for unstable lasers

M. V. BERRY

H. H. Wills Physics Laboratory, Tyndall Avenue, Bristol BS8 1TL, UK

(*Received 19 November 2001*)

Abstract. The linewidth of an unstable laser exceeds the quantum minimum by the Petermann factor K, which depends on the overlap between left and right eigenvectors of the (non-unitary) round-trip wave operator. When K is plotted as a function of the Fresnel number N, strong resonances occur, which are associated with degeneracies N_c lying close to the real axis in the complex N plane. For certain values of the magnification, degeneracies can lie on the real axis, and K is infinite. The Horwitz–Southwell asymptotic theory of the spectrum, presented here in a very accurate form and with a streamlined derivation, is used to show that the peaks occur near $N = s - \frac{1}{8}$ (s integer), and to give reliable formulae for the resonance widths Im N_c and other features of the degeneracies. Low-lying resonances have discontinuous profiles associated with mode switching where the absolute values of the eigenvalues cross (these are not degeneracies).

1. Introduction

Unstable lasers, for example the confocal laser illustrated in figure 1, are different from the more familiar stable lasers in several respects. For example, their mode profiles (graphs of intensity as a functon of position) are fractals, and this feature has been the subject of recent discussion [1–6].

My main purpose here is to explain a different aspect of unstable lasers, namely the fact that their linewidth can be enormously greater than that of stable lasers. This is quantified by the Petermann excess-noise factor K (section 2); New [7] has given an excellent account of the physical meaning and origin of K. The unusual properties emerge when K is considered as a function of the equivalent Fresnel number [8]

$$N = \frac{a^2}{2\lambda_0 L}(M-1), \tag{1}$$

where, referring to figure 1, the cavity has mirrors separated by L, with focal lengths f_1 and f_2 defining the magnification $M = f_1/f_2$, $2a$ is the width of the small (feedback) mirror and λ_0 is the wavelength of the light. Although N is defined as real by equation (1), it will be mathematically continued into the complex plane in subsequent analysis.

As N increases, K increases on the average and also exhibits large peaks, separated by $\Delta N \approx 1$. I shall show numerically (section 4) and analytically (section

Journal of Modern Optics ISSN 0950–0340 print/ISSN 1362–3044 online © 2003 Taylor & Francis Ltd
http://www.tandf.co.uk/journals
DOI: 10.1080/09500340210135402

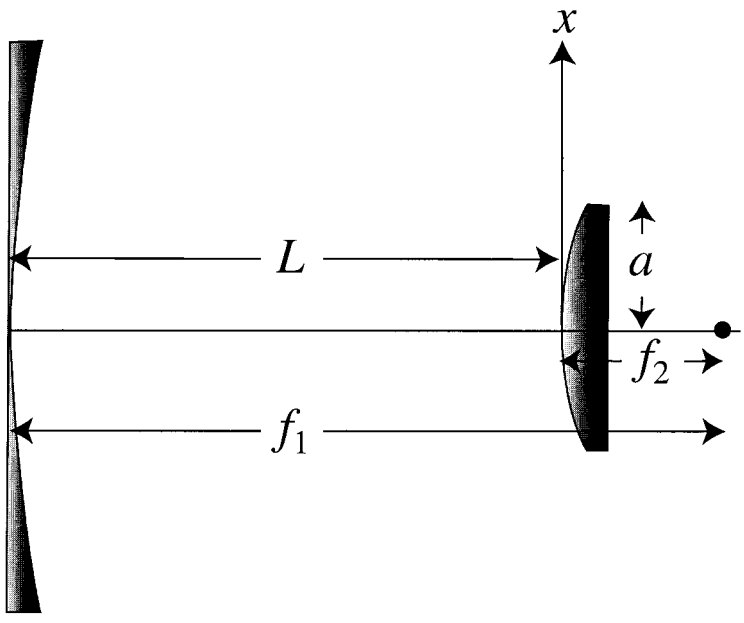

Figure 1. Strip resonator cavity corresponding to a confocal unstable laser.

5) that these peaks are resonances, associated with degeneracies where the complex lowest-loss mode eigenvalue γ is degenerate with that of the next-lowest-loss mode. The degeneracies occur at points N_c in the complex N plane, near $N = s - \frac{1}{8}$ (s integer) on the real axis and close to a curve whose form will be calculated explicitly. For general magnification M, there is zero probability that degeneracies will occur precisely on the real axis. However, for certain values of M, one of which is given explicitly, this can occur, and then $K \to \infty$.

It is important to distinguish degeneracies from eigenvalue crossings, which occur on the real N axis close (once again) to the points $N = s - \frac{1}{8}$. Whereas the lowest- and next-lowest-loss mode eigenvalues are identical at the degeneracies, only their moduli $|\gamma|$ coincide at the crossings [8, 9]. It must be stressed that it is the *degeneracies*, and not the crossings, that are responsible for the large values of the Petermann factor. The crossings give rise to peculiar resonance shapes for small N (section 6).

This theory of K will be derived with the aid of a slight modification (section 3) of a beautiful and powerful large-N asymptotic theory of unstable laser modes, created by Horwitz [9] and Southwell [10]. Two subsidiary purposes of this paper are to give a derivation of this asymptotic theory that displays its structure in a simple way, and to demonstrate its very high accuracy, even for $N \approx 1$. In some numerical applications, versions of the Horwitz–Southwell theory have been used as the basis of further refinements (e.g. by iteration), but the version here is so accurate that this is not necessary.

From a mathematical point of view, unstable lasers are interesting because their characteristic properties depend on the fact that the operator governing their modes is non-unitary. As will become clear, the contrast with unitary operators becomes extreme in the neighbourhood of degeneracies. Therefore K essentially embodies the physics of non-unitarity, and, because the degeneracies dominating

K occur for complex N, the Petermann factor represents 'real physics in the complex plane'. Excess noise joins a growing group of phenomena depending on degeneracies of non-unitary (or non-Hermitian) operators. Others include propagation near the optic axes of absorbing anisotropic crystals [11, 12], and the diffraction of atomic beams by crystals of light [13, 14].

To bring out the main ideas as clearly as possible, the theory of this paper is restricted to strip resonators, where (figure 1) the cavity is two dimensional and the mirrors are one dimensional. Calculations for more realistic three-dimensional cavities [15] have shown that K depends strongly on the shape of the mirrors. However, the underlying reason for the large values of K is the same as for strip resonators, namely degeneracies.

2. Basics

The lowest-loss mode profile $u(x)$ in any plane, for example close to the small mirror, can be regarded as an eigenvector $|u\rangle$ of an operator $\hat{T}$ representing wave propagation in a round trip of the cavity:

$$\hat{T}|u\rangle = \gamma|u\rangle, \quad \langle x\,|\,u\rangle \equiv u(x). \tag{2}$$

For unstable lasers, losses at the edges of the mirrors make $\hat{T}$ non-unitary, so that $|\gamma| < 1$. Therefore its right eigenvectors $|u\rangle$ are different from the left eigenvectors $\langle v|$, defined, together with the corresponding profile $v(x)$, by

$$\langle v|\hat{T} = \gamma\langle v|, \qquad \langle v|x\rangle \equiv v(x),$$

that is

$$\hat{T}^{\dagger}|v\rangle = \gamma^{*}|v\rangle, \qquad \langle x|v\rangle = v^{*}(x). \tag{3}$$

The Petermann factor that will be the focus of our interest here can now be defined in terms of the 'self-overlap' between the right and left eigenvectors, by

$$K = \frac{\langle u\,|\,u\rangle\langle v\,|\,v\rangle}{|\langle u\,|\,v\rangle|^{2}}. \tag{4}$$

Here and hereafter we shall measure positions in the plane of the feedback mirror in units of a. Then the explicit form of the round-trip operator is [8]

$$\langle\, x\,|\,\hat{T}|y\rangle = \left(\frac{2N}{\mathrm{i}(M - M^{-1})}\right)^{1/2} \exp\left[\mathrm{i}\frac{2\pi N}{1 - M^{-2}}\left(y - \frac{x}{M}\right)^{2}\right]\Theta(1 - |y|), \tag{5}$$

where Θ denotes the unit step (without this step, cutting off the reflection at the edges of the mirror, $\hat{T}$ would be unitary). (Although equation (5) is written for a confocal laser, the operator for any unstable laser can be written in the same form, after a simple transformation involving a phase factor quadratic in x.)

From the integral equation (12) below corresponding to equation (5), elementary manipulations show that for this particular operator $v(x)$ and $u(x)$ are related by [16]

$$v(x) = u(x)\exp\left(2\pi\,\mathrm{i}Nx^{2}\right)\Theta(1 - |x|). \tag{6}$$

Thus $v(x)$ is non-zero only in the interval $|x| < 1$ corresponding to the mirror, unlike $u(x)$ whose domain extends outside the mirror, that is for $|x| > 1$. Never-

theless, the normalization of $u(x)$, that occurs in the definition (4) of K, can be expressed as an integral only over the interval $|x| < 1$; in appendix A it is shown that

$$\langle v|v\rangle = \int_{-1}^{1} \mathrm{d}x|u(x)|^2, \quad \langle u|u\rangle = \int_{-\infty}^{\infty} \mathrm{d}x\,|u(x)|^2 = \frac{1}{|\gamma|^2}\int_{-1}^{1} \mathrm{d}x\,|u(x)|^2. \tag{7}$$

Thus the Petermann factor can be written in the form

$$K = \frac{\left(\int_{-1}^{1} \mathrm{d}x|u(x)|^2\right)^2}{|\gamma|^2\left|\int_{-1}^{1} \mathrm{d}x\,u^2(x)\exp\left(2\pi\mathrm{i}Nx^2\right)\right|^2}. \tag{8}$$

If the operator $\hat{T}$ were unitary, we would have $v(x) = u^*(x)$ and $|\gamma| = 1$, and the self-overlap in equation (4), and hence K, would both be unity. The extreme antithesis occurs at degeneracies; there the self-overlap is zero, and so K is infinite. To see this, and to motivate our later emphasis on degeneracies, consider the general 2×2 matrix

$$\mathbf{T} = \begin{pmatrix} a & b \\ c & d \end{pmatrix}, \tag{9}$$

where a, b, c and d can be complex. Labelling the two states $+$ and $-$, the eigenvalues are

$$\gamma_{\pm} = \tfrac{1}{2}(a + d \pm \varepsilon), \quad \varepsilon = \gamma_+ - \gamma_- = [(a-d)^2 + 4bc]^{1/2}, \tag{10}$$

where ε denotes the eigenvalue difference, so that a degeneracy corresponds to $\varepsilon = 0$. In appendix B it is shown that near a degeneracy the self-overlap (the same for both normalized states for a 2×2 matrix) is

$$|\langle v|u\rangle| \to \frac{|\varepsilon|}{|b| + |c|} \quad \text{as} \quad \varepsilon \to 0. \tag{11}$$

Thus $|u\rangle$ and $\langle v|$ become orthogonal at a degeneracy, and K indeed diverges. Later we shall explore the full consequences of this.

3. Reprise of Horwitz–Southwell asymptotics

Corresponding to the operator equation (2) is the integral equation

$$\gamma u(x) = \langle x|\hat{T}|u\rangle = \left(\frac{2N}{\mathrm{i}(M - M^{-1})}\right)^{1/2}\int_{-1}^{1} \mathrm{d}y \exp\left[\mathrm{i}\frac{2\pi N}{1 - M^{-2}}\left(y - \frac{x}{M}\right)^2\right]u(y), \tag{12}$$

which will be the basis of our subsequent analysis. To obtain a preliminary orientation, consider the crude approximation of taking $u(x)$ as a constant and regarding the limits of integration as infinite. This gives

$$u(x) \sim 1, \quad \langle x|\hat{T}|u\rangle \sim \frac{1}{M^{1/2}},$$

and so

$$\gamma \sim \frac{1}{M^{1/2}}, \tag{13}$$

motivating the definition of the scaled eigenvalue λ, defined by

$$\gamma \equiv \frac{\lambda}{M^{1/2}}. \tag{14}$$

Horwitz [9] asymptotics is based on the mathematical observation that for large N the integrand in equation (12) oscillates rapidly, and the main contributions come from any stationary-phase points in the range of integration $|x| < 1$, and from the end points $x = \pm 1$. Southwell [10] asymptotics is based on the physical counterpart of these observations, namely that the self-reproducing mode is generated by geometrical reflections, and by waves diffracted from the edges of the mirror.

To incorporate the above observations into a consistent theory, in which the mode u is built up from iteration of equation (12), starting from $u_0(x) = 1$, we define the set of functions (motivated by the iteration to follow)

$$\begin{aligned} G_n(x) = \frac{1}{2\pi}\left(\frac{\mathrm{i}(1-M^{-2n})}{2n}\right)^{1/2} \\ \times \left(\frac{\exp\{\mathrm{i}[2\pi N/(1-M^{-2n})](1-x/M^n)^2\}}{1-x/M^n}\right. \\ \left. + \frac{\exp\{\mathrm{i}[2\pi N/(1-M^{-2n})](1+x/M^n)^2\}}{1+x/M^n}\right). \end{aligned} \tag{15}$$

Physically, the two terms in G_n represent waves diffracted by the two edges of the small mirror, after n geometrical reflections. It might seem surprising that the edge waves are given by this elementary trigonometric formula, rather than by the more familiar Fresnel integral [17]. The simplicity of equation (15) rests on the convenient fact that for these multiply reflected waves the shadow boundaries, whose description would require the full Fresnel integral, lie outside the interval $|x| < 1$ where we need $u(x)$; so the trigonometric approximation suffices.

Elementary algebra, some of whose details are given in appendix C, now gives the result of the action on the initial state 1 of the integral operator in equation (12):

$$\left(\frac{2N}{\mathrm{i}(1-M^{-2})}\right)^{1/2}\int_{-1}^{1} \mathrm{d}y \exp\left[\mathrm{i}\frac{2\pi N}{1-M^{-2}}\left(y-\frac{x}{M}\right)^2\right]1 \approx 1 - G_1(x). \tag{16}$$

Here the approximation sign $\approx$ means that the integral is evaluated by including only the lowest-order stationary-phase contribution (first term on the right-hand side), corresponding to geometrical reflection, and the lowest-order edge-wave contributions (second term on the right-hand side), corresponding to edge waves. The action of the integral operator acting on G_n, in the same approximation, is

$$\left(\frac{2N}{\mathrm{i}(1-M^{-2})}\right)^{1/2}\int_{-1}^{1} \mathrm{d}y \exp\left[\mathrm{i}\frac{2\pi N}{1-M^{-2}}\left(y-\frac{x}{M}\right)^2\right]G_n(y) \approx G_{n+1}(x) - G_n(1)G_1(x), \tag{17}$$

where again the first and second terms on the right-hand side correspond to geometrically reflected and edge-diffracted waves respectively.

These two equations can be regarded as approximations to the integral operator $\hat{T}$. It is remarkable that the corresponding eigenequation, approximating equation (12), can be solved exactly (appendix C), with the result that the modes even in x are given by

$$u(x) = 1 - \sum_{n=1}^{\infty} \frac{G_n(x) - G_n(1)}{\lambda^n}, \tag{18}$$

where the scaled eigenvalues λ are the solutions of

$$P(\lambda, N) = \lambda - 1 + G_1(1) + \sum_{n=1}^{\infty} \frac{G_{n+1}(1) - G_n(1)}{\lambda^n} = 0. \tag{19}$$

The function $P(\lambda, N)$ is essentially the determinant of the (approximated) operator (5). The lowest-loss mode is the one (or two, in the case of a crossing) with the largest value of $|\lambda|$.

The series in equations (18) and (19) are very convenient for numerical evaluation, because they converge very rapidly, as can be seen from the asymptotic forms

$$\begin{aligned} G_n(1) &\approx \frac{\exp[2\pi i(N+\frac{1}{8})]}{\pi(2N)^{1/2}} \cos\left(\frac{4\pi N}{M^n}\right) \text{ if } n \gg 1 \text{ or } M \gg 1, \\ G_\infty(1) = G_\infty(x) &= \frac{\exp[2\pi i(N+\frac{1}{8})]}{\pi(2N)^{1/2}}. \end{aligned} \tag{20}$$

The number of terms required for convergence is of the order of

$$m_{\max} = \frac{\log N}{\log M}. \tag{21}$$

Note the factors $\exp[2\pi i(N+\frac{1}{8})]$; these are positive real whenever $N = s - \frac{1}{8}$, values close to the maxima of K, as will be shown later.

Figure 2 shows the Petermann factor for the lowest-loss mode, for rather small values of N. The computations were made according to equation (8), in two ways:

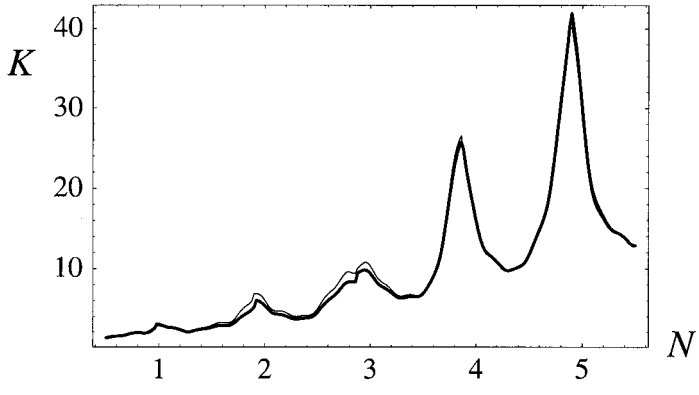

Figure 2. Petermann factor for the lowest-loss mode, for $M = 1.5$, computed exactly, by matrix diagonalization (——), and according to the asymptotic theory (——).

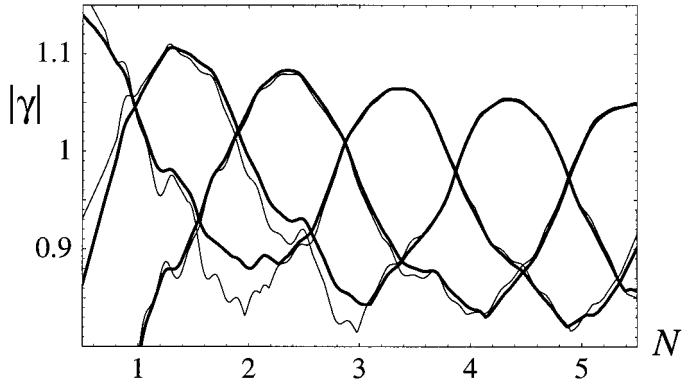

Figure 3. Eigenvalues $|\gamma|$ for the three lowest-loss modes, for $M = 1.5$, computed exactly (——), and by the asymptotic theory (——).

firstly, using the exact modes, calculated by diagonalizing the matrix obtained by discretizing the integral operator in equation (12) and, secondly, using the approximate modes (18). The large values near $N = s - \frac{1}{8}$, which we seek to explain, are clear, as is the excellent agreement, improving as N increases, between the asymptotic and exact theories. Figure 2 also agrees very closely with a previously published exact calculation [16]. The corresponding spectra, in the form of absolute values $|\gamma|$ of the eigenvalues for the three lowest-loss modes, are shown in figure 3; again the asymptotic theory improves with increasing N, especially for the lowest-loss mode that is our main interest here. More discriminating are the eigenfunctions $u(x)$, whose absolute values are shown in figure 4; again the asymptotic theory gives excellent agreement with exact calculations. Further calculations, not reported here, confirm the accuracy of the asymptotic theory. One example is $M = 1.9$, $N = 49.4$, for which New [7] calculated $K \approx 290$ from the exact round-trip wave map; from the asymptotic theory, we obtain $K = 289.477$. Thus we can have full confidence in a theory of the resonances based on the asymptotic theory.

4. Fine structure of degeneracies

According to equation (10), a degeneracy, that is vanishing ε, requires both the real and the imaginary parts of the square root in equation (10) to vanish; therefore degeneracies have codimension two, a result that holds for a general complex matrix. This implies that degeneracies are infinitely unlikely to occur as a single real parameter, for example N, is varied, but can occur in the complex plane of N. Equations (4) and (11) then show that K will diverge as $1/|\varepsilon|^2$. Now we shall examine this behaviour in detail.

Let a degeneracy occur at the complex Fresnel number $N = N_c$ where the scaled eigenvalue is λ_c. This situation corresponds to a double zero of the determinant function $P(\lambda, N)$, given by equation (19) according to the asymptotic theory. Thus (denoting derivatives by ∂)

$$P(\lambda_c, N_c) = 0 \quad \text{and} \quad \partial_\lambda P(\lambda_c, N_c) = 0, \; N_c = N_{c1} + iN_{c2}. \tag{22}$$

Expanding about λ_c, N_c to lowest order gives

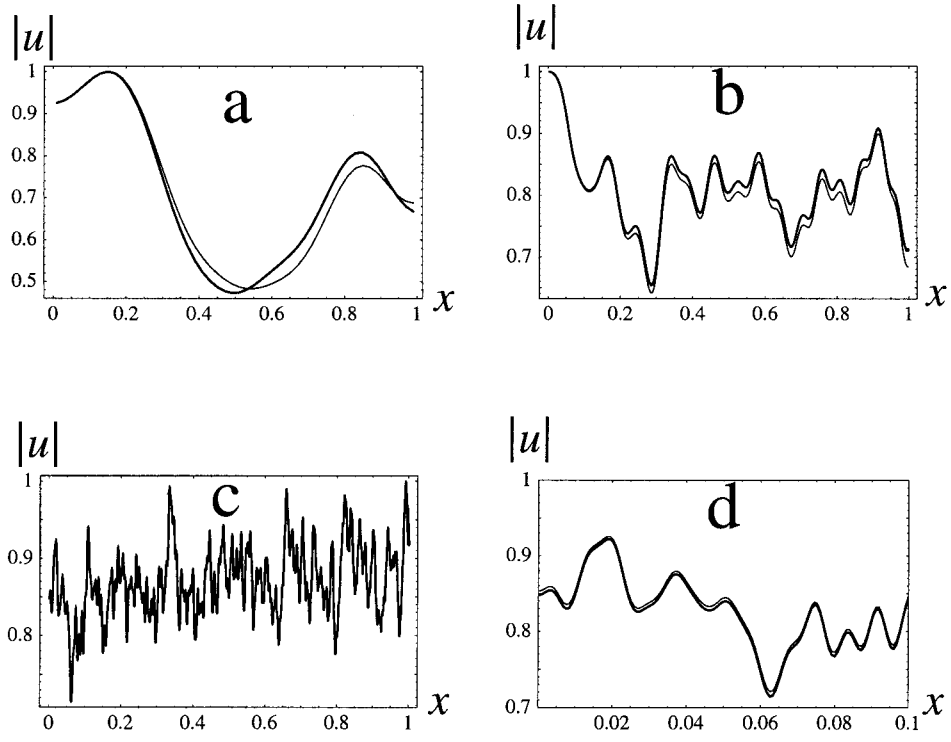

Figure 4. Lowest-loss eigenfunctions $|u(x)|$ for $M = 1.5$, computed exactly (——), and by the asymptotic theory (——), for (*a*) $N = 1$, (*b*) $N = 5$ and (*c*) $N = 50$; (*d*) magnification of (*c*).

$$P(\lambda_c + \Delta\lambda, N_c + \Delta N) = \tfrac{1}{2}(\Delta\lambda)^2 \partial_\lambda^2 P(\lambda_c, N_c) + \Delta N \partial_\lambda P(\lambda_c, N_c) + \cdots = 0, \quad (23)$$

and hence the lowest-order behaviour of the eigenvalue separation near N_c:

$$\begin{aligned} \lambda_+ - \lambda_- &\to 2\Delta\lambda \\ &\to 2\left(-2\frac{\partial_N P}{\partial_\lambda^2 P}(N - N_c)\right)^{1/2} \\ &\equiv C(N - N_c)^{1/2} \text{as } N \to N_c. \end{aligned} \quad (24)$$

In section 5 we will derive an approximation for the constant C.

From equation (24) we regain the well-known generalization of the 2×2 result (10), that a degeneracy is a square-root branch point of the spectrum [18]. According to equation (11) a degeneracy is also a branch point of the self-overlap. To explore this behaviour numerically, it is necessary to determine the location of degeneracies. The local analytic branch-point structure is the basis of a simple and accurate method for locating degeneracies, described in appendix D. More than 800 degeneracies were determined in this way and form the basis of the numerical experments now to be described.

As was previously asserted and as will be justified in section 5, degeneracies occur near $N = s - \frac{1}{8}$. Figure 5 (*a*) shows a path in the complex N plane starting at this value of N and passing through the nearest degeneracy N_c, and figures 5 (*b*) and 5 (*c*) show the behaviour of the self-overlap and the eigenvalue separation along this path, calculated exactly and with the asymptotic theory. The branch-point behaviour of both functions is evident, as is the high accuracy of the asymptotic theory.

For degeneracies close to the real N axis, it is natural to approximate K using a resonance model suggested by (11), based on the local branch-point structure, namely

$$K(N) \approx K_{\text{resonance}}(N) = \frac{K_{\max}|N_{c2}|}{|N - N_c|} = \frac{K_{\max}|N_{c2}|}{[(N - N_{c1})^2 + N_{c2}{}^2]^{1/2}} \quad \text{for } N \text{ close to integer} - \tfrac{1}{8}. \tag{25}$$

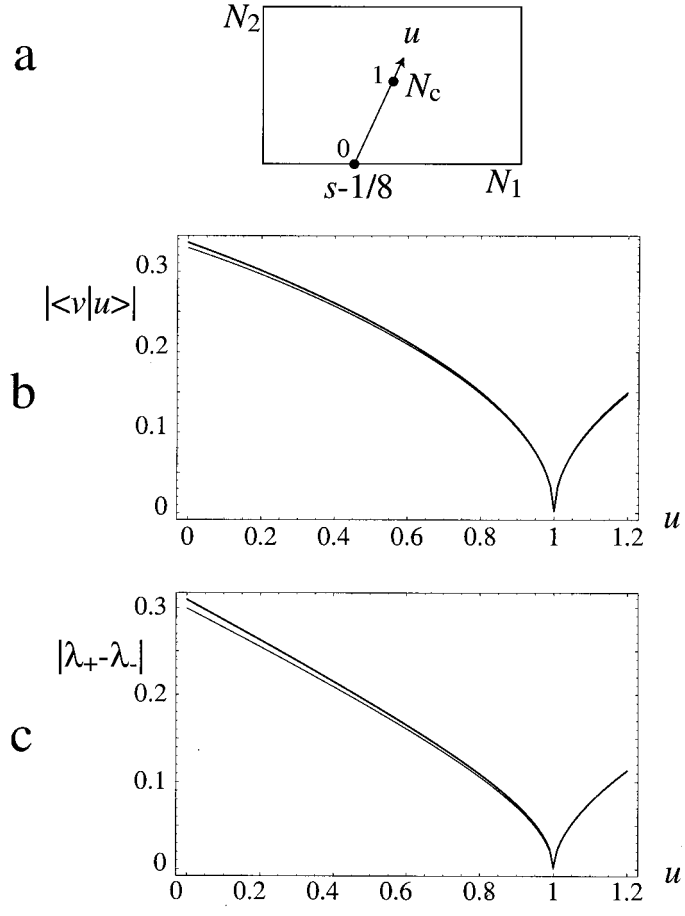

Figure 5. (*a*) Path in the complex N plane passing through a degeneracy N_C; (*b*) corresponding behaviour of the self-overlap $|\langle v|u\rangle|$, calculated exactly (——) and with the asymptotic approximtion (——), for $M = 1.5$; (*c*) as (*b*), but for the eigenvalue difference $|\lambda_+ - \lambda_-|$.

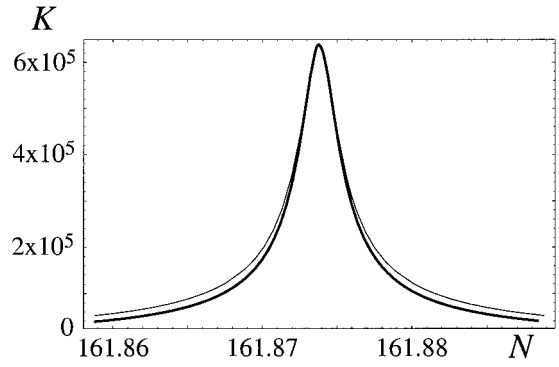

Figure 6. Petermann factor near the $s = 162$ resonance, calculated for $M = 1.5$ from the full asymptotic theory (——) and from the local resonance model (25) (——).

Figure 6 shows that this 'square root of Lorentzian' form accurately describes both the width and the shape of the Petermann factor where this takes very large values. From figure 2 it appears that the low-lying resonances have a different form; this will be explained in section 6.

5. Asymptotics of degeneracies

The leading-order large-N behaviour of the Petermann factor can be obtained easily, by substituting into equation (8) the lowest-order approximations for $u(x) \sim 1$ and $\gamma \approx 1/M^{1/2}$ (cf. equation (13)). Thus

$$K \approx \frac{4M}{\left|\int_{-1}^{1} \mathrm{d}x \exp(2\pi \mathrm{i} N x^2)\right|^2} \approx 8NM. \tag{26}$$

However, this formula fails completely to capture the resonance peaks that dominate K for intermediate values of N. As we have seen (figures 2 and 6) these peaks are captured by numerically integrating, according to equation (8), the modes (18) given by the asymptotic theory. By further approximating the asymptotic theory, it is possible to obtain more explicit information about the resonances.

To accomplish this, we replace summation by integration in the eigenvalue equation (19), replacing $G_n(1)$ by its large-n approximation (20). Thus, in equation (19), with $n^* \to \infty$,

$$\begin{aligned} G_1(1) + \sum_{n=1}^{\infty} \frac{G_{n+1}(1) - G_n(1)}{\lambda^n} &= (\lambda - 1) \sum_{n=1}^{n^*} \frac{G_n(1)}{\lambda^n} + \frac{G_\infty(1)}{\lambda^{n^*}} \\ &\approx (\lambda - 1) \int_1^\infty \mathrm{d}n \, \frac{G_n(1)}{\lambda^n} \\ &\approx G_\infty \frac{\cos[(\pi \log \lambda)/(2 \log M)]}{\lambda^{\log(4\pi N)/(\log M)}} (\lambda - 1) \Gamma\left(\frac{\log \lambda}{\log M}\right). \end{aligned} \tag{27}$$

Incorporating the fact that λ is close to unity, we obtain the following approximate form for the asymptotic function (determinant of the round-trip wave operator) whose vanishing gives the eigenvalues:

$$P(\lambda, N) \approx \lambda - 1 + \frac{\exp[2\pi i(N + \frac{1}{8})]}{\pi(2N)^{1/2}} \exp\left(-(\lambda - 1)\frac{\log(4\pi N)}{\log M}\right) = 0. \tag{28}$$

At a degeneracy, the derivative must vanish as well (cf. equation (22)); so we also need

$$\partial_\lambda P(\lambda, N) \approx 1 - \frac{\log(4\pi N)}{\log M} \frac{\exp\left([2\pi i\left(N + \frac{1}{8}\right)\right]}{\pi(2N)^{1/2}} \exp\left(-(\lambda - 1)\frac{\log(4\pi N)}{\log M}\right) = 0. \tag{29}$$

These equations are easy to solve to lowest relevant orders in $1/N$. For the degenerate eigenvalue, they give, for the degeneracy labelled by the integer s,

$$\lambda_c \approx 1 - \frac{\log M}{\log[4\pi(s - \frac{1}{8})]}, \tag{30}$$

and, for the positions of the resonances in the complex N plane,

$$N_c = N_{c1} + iN_{c2} \approx s - \tfrac{1}{8} + i\delta\left(s - \tfrac{1}{8}\right), \tag{31}$$

where

$$\delta(N) = \frac{1}{2\pi} \log\left(\frac{e \log(4\pi N)}{\pi(2N)^{1/2} \log M}\right). \tag{32}$$

The predictions of these simple formulas can be compared with those of the full asymptotic theory (which, as we have seen, are almost indistinguishable from exact matrix computations). Figure 7 shows that apart from a small shift the trend of the eigenvalues is accurately reproduced by equation (30). An unexpected implication of the approximation (30) is that the degenerate eigenvalues are almost real, and figure 8 shows that this is the case.

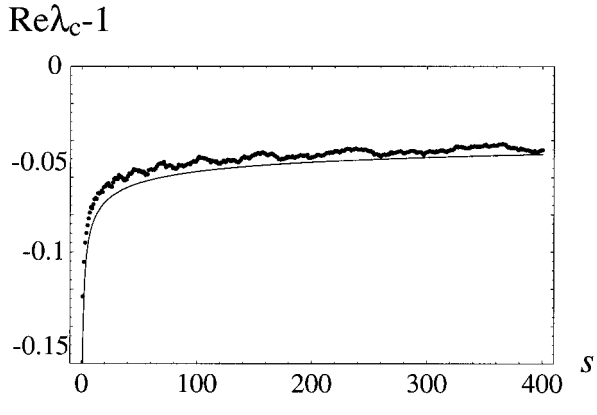

Figure 7. Re $\lambda_c - 1$ versus s for 400 degeneracies for $M = 1.5$, calculated from the full asymptotic theory of section 3 (·), and from the theory (equation (30)) (——).

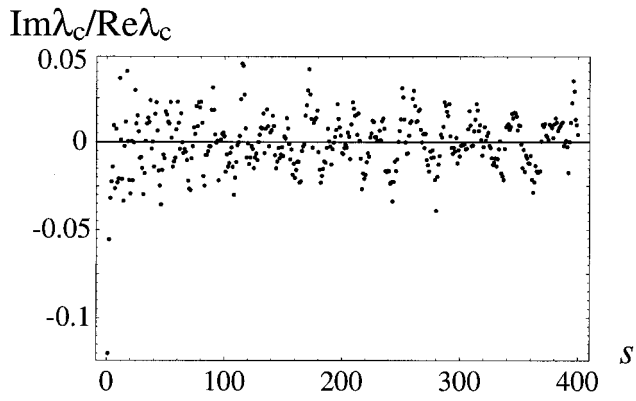

Figure 8. As figure 7, but for $(\mathrm{Im}\ \lambda_c)/(\mathrm{Re}\ \lambda_c)$, for which the theoretical prediction is zero.

The most important application of this approximate version of the asymptotic theory is to predict, according to equations (31) and (32), the locations N_c of the complex degeneracies, especially their imaginary parts N_{c2} which give the widths of the resonances. Figure 9 illustrates how well the degeneracies are given by this theory. Particularly interesting are degeneracies close to the real axis, for which the Petermann factors are largest. According to equation (32), these occur close to values of N where δ vanishes, given by the solution of

$$\frac{e\log(4\pi N)}{\pi(2N)^{1/2}\log M} = 1. \tag{33}$$

For $M = 1.5$, this critical value of N is 122.70 (the dependence on M is sensitive: for $M = 1.1$ and $M = 3$, the critical values of N are 5036.61 and 5.62 respectively).

The degeneracies N_c are scattered erratically close to the predictions (31) and (32) of the approximate asymptotic theory. For fixed M, it is infinitely improbable that one of the N_c is exactly real, but, as M varies, the degeneracies will move continuously; so the trajectory of one or more of them, close to the critical N given by the solution of equation (33), can cross the real axis. Then $K = \infty$, an

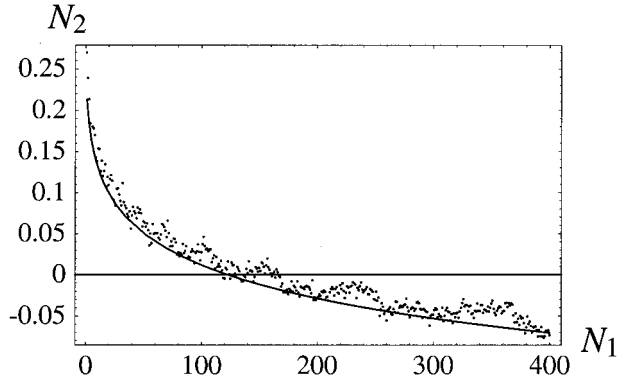

Figure 9. The first 400 degeneracies in the complex N plane for $M = 1.5$, calculated from the full asymptotic theory of section 3 (·), and from the (equations (31) and (32)) (——).

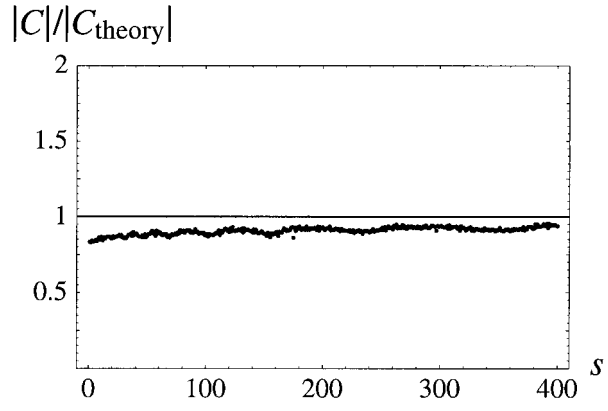

Figure 10. Coefficient $|C|/|C_{\text{theory}}|$ in the branch-point law (24), with the theory (equation (34)), for eigenvalue separation near the first 400 degeneracies, for $M = 1.5$.

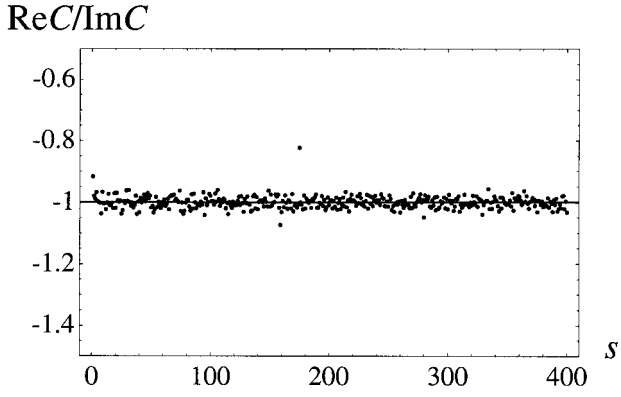

Figure 11. As figure 10, but for (Re C)/(Im C), for which the theoretical value is -1.

intriguing possibility worth exploring experimentally. An explicit example occurs for $M = 2.901$, $N = 3.898$ (this is calculated with the exact wave operator; the full asymptotic theory gives $M = 2.911$, $N = 3.896$).

As N increases beyond the critical value given by the solution of equation (33), the degeneracies recede from the real axis and the Petermann peaks become smaller. For still larger values of N, the peaks are replaced by gentle oscillations, until ultimately the limiting form (26) is attained, with K increasing monotonically.

A final application of the approximate asymptotic theory is to the calculation of the constant C in the branch-point law (24) for the eigenvalue separation near a degeneracy. The required derivatives of $P(\lambda, N)$ are easily calculated from equation (28) and give

$$C \approx 4\frac{\log M}{\log(4\pi N)}(-\mathrm{i}\pi)^{1/2}. \tag{34}$$

Figure 10 shows that the modulus $|C|$ is close to this predicted value, and figure 11 shows that the ratio (Re C)/(Im C) is close to -1, as predicted by the factor $(-\mathrm{i})^{1/2}$.

6. Resonance switching

Although it is clear from figure 6 that the resonance formula (25) is capable of giving a very accurate description of the shapes of the Petermann peaks, this theory seems to fail for the lowest resonances in figure 2. Magnification of these low-lying peaks (figure 12) confirms that their shapes are indeed different, and that the asymptotic theory still gives a reasonable approximation, even for these low values of N, and also indicates that the K can be a discontinuous function of N.

As has been recognized before [16], the origin of the peculiar shapes for small N lies in the mathematically inessential but physically important fact that Krefers to the lowest-loss mode. This applies in particular to the discontinuities, which occur at crossings of the eigenvalue modulus $|\gamma|$ (figure 2). We temporarily label the two states near the crossing by 1 and 2, such that each is a continuous function of (real) N through the crossing N_{cross} (which as we have seen is not a degeneracy), implying that $\langle v_1|u_1\rangle$ and $\langle v_2|u_2\rangle$ are also continuous functions of N. Then, as N increases through N_{cross}, the lowest-loss state switches from 1 to 2 or vice-versa, so that the self-overlaps, and hence K, also switch.

This phenomenon of resonance switching cannot be modelled by a 2×2 matrix because, as a short calculation shows, $|\langle v_1|u_1\rangle| = |\langle v_2|u_2\rangle|$ identically, even far from the degeneracy: in order for the self-overlaps to be different, the states 1 and 2 must be embedded in a larger matrix. Numerical explorations confirm that resonance switching can occur in 3×3 matrices. A simpler phenomenological model is provided by a degeneracy sufficiently far from the real axis for its shadows on the real axis, for the states 1 and 2, to have separated and to have acquired different strengths. If these shadows are centred at $x = \pm a$, with equal widths 1

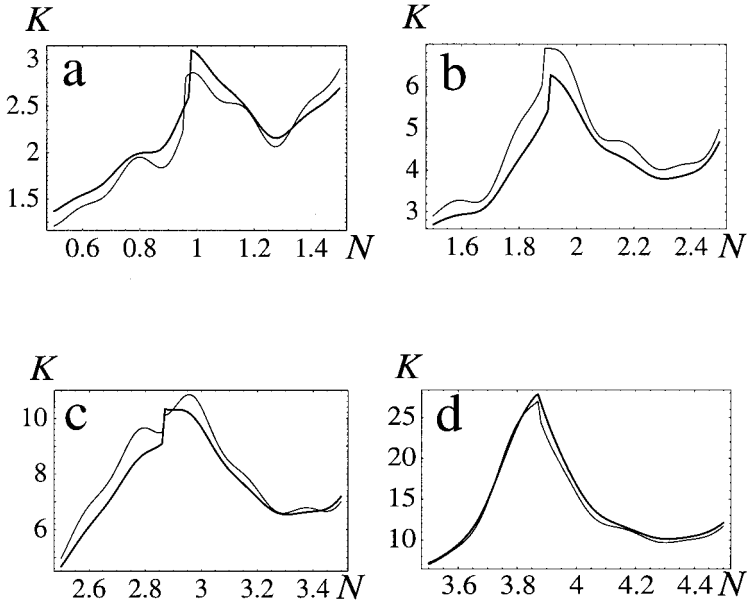

Figure 12. Magnification of lowest resonances for $M = 1.5$, calculated exactly (——) and according to the asymptotic theory (——), for (*a*) $s = 1$, (*b*) $s = 2$, (*c*) $s = 3$ and (*d*) $s = 4$, showing resonance switching at crossings of $|\gamma|$.

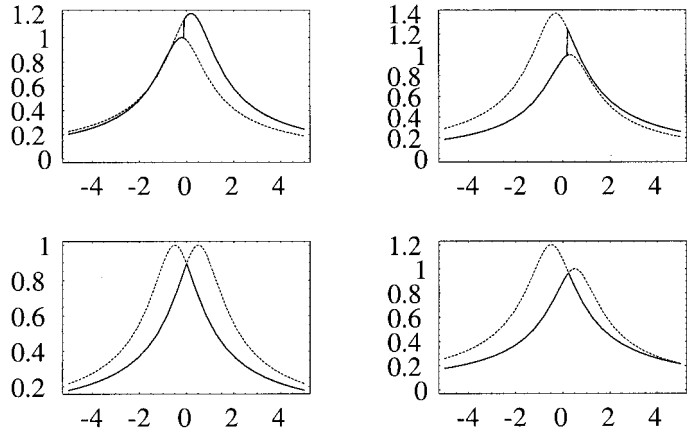

Figure 13. Profiles calculated from the resonance switching model $R(x)$ (——), with the underlying continuous resonances (· · · · ·), for several choices of parameters in equation (35).

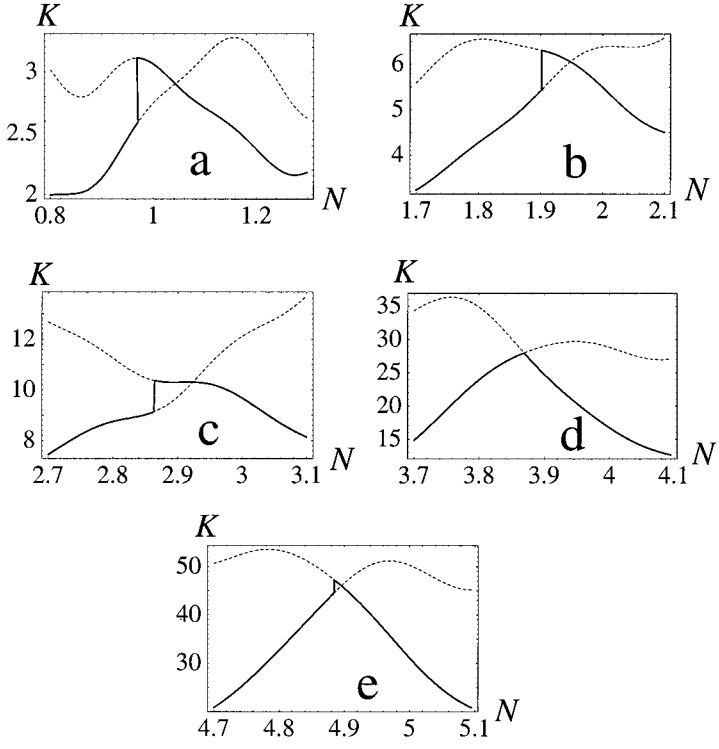

Figure 14. Petermann factors for lowest-loss mode (——) and the next-to-lowest-loss mode (· · · · ·) for $M = 1.5$, for (*a*) $s = 1$, (*b*) $s = 2$, (*c*) $s = 3$, (*d*) $s = 4$ and (*e*) $s = 5$, showing continuity of the underlying self-overlaps.

and strengths 1 and b, and if the eigenvalue moduli switch at x_{cross}, then the model is

$$R(x) = \frac{\Theta(x - x_{\text{cross}})}{[(x-a)^2+1]^{1/2}} + \frac{b\Theta(x_{\text{cross}} - x)}{[(x+a)^2+1]^{1/2}}. \tag{35}$$

As figure 13 shows, for different choices of a, b and x_{cross} the model is capable of generating discontinuous profiles resembling those of the calculated Petermann factors.

The continuity of the underlying overlaps can be confirmed by superposing Petermann profiles calculated for the lowest-loss mode and the next-to-lowest-loss mode (figure 14) (see also [16]). The individual resonances are evident, except for $s = 3$ where they are too broad.

For sufficiently large values of N (that depend on M), crossings of $|\gamma|$ no longer occur [9]; so the phenomenon of resonance switching no longer occurs and is replaced by the canonical behaviour illustrated in figure 6.

Acknowledgments

I am indebted to Professor Brian Dalton for introducing me to this problem, to Professor Geoffrey New for helping me to understand the Horwitz–Southwell theory, and to the Physics Department of the Technion, Israel, where the first draft of this paper was written.

Appendix A: Mode normalization identity

This is the derivation of the last equality in equation (7). From the integral equation (12), we have

$$\begin{aligned}\int_{-\infty}^{\infty} \mathrm{d}x\,|u(x)|^2 &= \frac{1}{|\gamma|^2}\frac{2N}{(M-M^{-1})}\int_{-\infty}^{\infty}\mathrm{d}x\int_{-1}^{1}\mathrm{d}y_1\int_{-1}^{1}\mathrm{d}y_2 \\ &\quad\times u^*(y_1)u(y_2)\exp\left[\mathrm{i}\frac{2\pi N}{1-M^{-2}}\left(y_2^2-y_2^2-\frac{2x}{M}(y_2-y_1)\right)\right] \\ &= \frac{1}{|\gamma|^2}\int_{-1}^{1}\mathrm{d}y_1\int_{-1}^{1}\mathrm{d}y_2 u^*(y_1)u(y_2)\delta(y_2-y_1) \\ &= \frac{1}{|\gamma|^2}\int_{-1}^{1}\mathrm{d}y|u(y)|^2, \end{aligned} \tag{A 1}$$

Q.E.D.

Appendix B: Self-overlap near a degeneracy

This is the derivation of equation (11). For the matrix (9), the left and right eigenvectors are

$$|u\rangle = \frac{1}{(|b|^2+|\gamma-a|^2)^{1/2}}\begin{pmatrix} b \\ \gamma-a\end{pmatrix}, \quad \langle v| = \frac{(c\ \gamma-a)}{(|c|^2+|\gamma-a|^2)^{1/2}}, \tag{B 1}$$

with the eigenvalues γ given by equation (10); so the self-overlap is

$$\langle v|u\rangle = \frac{bc+(\gamma-a)^2}{[(|b|^2+|\gamma-a|^2)(|c|^2+|\gamma-a|^2)]^{1/2}}. \tag{B 2}$$

For the numerator, we have, repeatedly using equation (10),

$$bc + (\gamma - a)^2 = bc + \tfrac{1}{4}(d - a \pm \varepsilon)^2$$
$$= \pm\tfrac{1}{2}\varepsilon(d - a) + \tfrac{1}{4}\varepsilon^2 \to \pm\varepsilon(-bc)^{1/2} \text{as } \varepsilon \to 0. \quad \text{(B 3)}$$

In the denominator, we have

$$|\gamma - a|^2 = \tfrac{1}{4}|d - a \pm \varepsilon|^2 \to \tfrac{1}{4}|d - a|^2 \to |bc|. \quad \text{(B 4)}$$

Thus

$$|\langle v|u\rangle| \to \frac{|\varepsilon\, bc|}{[(|c|^2 + |bc|)(|b|^2 + |bc|)]^{1/2}} = \frac{|\varepsilon|}{|b| + |c|}, \quad \text{(B 5)}$$

Q.E.D.

Appendix C: Asymptotic iteration algebra

This gives some details of the derivations of the iteration formulae (16) and (17) and the solution (18) and (19) of the approximate round-trip operator. The basic ingredient is the following standard result from the asymptotics of integrals [19] involving smooth functions $f(x)$ and $g(x)$, where N is a large parameter and $f(x)$ has a stationary point x_0 (i.e. $f'(x_0) = 0$) in the range of integration:

$$\int_{-1}^{1} \mathrm{d}x\, g(x) \exp[\mathrm{i}Nf(x)]$$
$$= \left(\frac{2\pi}{N|f''(x_0)|}\right)^{1/2} \exp(\mathrm{i}\{Nf(x_0) + \tfrac{1}{4}\pi \operatorname{sgn}[f''(x_0)]\})$$
$$+ \frac{1}{\mathrm{i}N}\left(\frac{g(1)}{f'(1)}\exp[\mathrm{i}Nf(1)] - \frac{g(-1)}{f'(-1)}\exp[\mathrm{i}Nf(-1)]\right) + \mathrm{O}\left(\frac{1}{N^{3/2}}\right). \quad \text{(C 1)}$$

The derivation of equation (16) is a straighforward application of equation (C1). The derivation of equation (17), although tedious in its details, is again straightforward, apart from one point. In the amplitude factor of the second term on the right-hand side of equation (17), representing the edge waves, it is necessary to approximate the factor $(1 \pm M^{-(n+2)})/(1 \pm M^{-n})$ by unity. This makes no discernible difference to the numerical results (cf. the evidence presented in figures 2–6), and is a negligible price to pay for the simplicity of equation (17), resulting in the exact solutions (18) and (19).

To derive equations (18) and (19), we write the mode in the form, inspired by (16) and (17),

$$u(x) = B - \sum_{n=1}^{n^*} \frac{G_n(x)}{\lambda^n}, \quad \text{(C 2)}$$

where $n^* \gg 1$ and then apply the approximate form (16) and (17) of the round-trip operator. The terms $G_n(x)$ cancel for $n > 1$, and equating coefficients of the terms in $G_1(x)$ gives

$$B = 1 + \sum_{n=1}^{n^*} \frac{G_n(1)}{\lambda^n}, \tag{C 3}$$

and hence the mode formula (18). Equating the constant terms now gives, after a little manipulation, the eigenvalue equation (19).

Appendix D: Determining degeneracies numerically

Corresponding to the branch-point behaviour (24) is

$$(\lambda_+ - \lambda_-)^2 \equiv L_2(N) \to C^2(N - N_c). \tag{D 1}$$

It follows that any N in this limiting region enables N_c to be determined from

$$N_c = N - \frac{L_2(N)}{\partial_N L_2(N)}. \tag{D 2}$$

In practice a good starting value is $N = s - \frac{1}{8}$ on the real axis. Application of equation (D2), with L_2 and its derivative evaluated numerically, gives a good approximation to N_c, and two further iterations gave sufficient accuracy for all the numercal explorations reported here.

References

[1] Karman, G. P., and Woerdman, J. P., 1998, Fractal structure of eigenmodes of unstable-cavity lasers, *Optics Lett.*, **23,** 1909–1911.
[2] Karman, G. P., McDonald, G. S., New, G. H. C., and Woerdman, J. P., 1999, Fractal modes in unstable resonators, *Nature*, **402,** 138.
[3] New, G. H. C., Yates, M. A., Woerdman, J. P., and McDonald, G. S., 2001, Diffractive origin of fractal resonator modes, *Optics Commun.*, **193,** 261–266.
[4] Courtial, J., and Padgett, M. J., 2000, Monitor-outside-a-monitor effect and self-similar fractal structure in the eigenmodes of unstable optical resonators, *Phys. Rev. Lett.*, **85,** 5320–5323.
[5] Berry, M. V., Storm, C., and van Saarloos, W., 2001, Theory of unstable laser modes: edge waves and fractality, *Optics Commun.*, **197,** 393–402.
[6] Berry, M. V., 2001, Fractal modes of unstable lasers with polygonal and circular mirrors, *Optics Commun.*, **200,** 321–330.
[7] New, G. H. C., 1995, The origin of excess noise, *J. mod. Optics*, **42,** 799–810.
[8] Siegman, A. E., 1986, *Lasers* (Mill Valley: University Science Books).
[9] Horwitz, P., 1973, Asymptotic theory of unstable resonator modes, *J. opt. Soc. Amr.*, **63,** 1528–1543.
[10] Southwell, W. H., 1986, Unstable-resonator-mode derivation using virtual-source theory, *J. opt. Soc. Amr.*, **3,** 1885–1891.
[11] Pancharatnam, S., 1955, The propagation of light in absorbing biaxial crystals—I. Theoretical, *Proc. Ind. Acad. Sci.*, **42,** 86–109.
[12] Berry, M. V., 1994, Pancharatnam, virtuoso of the Poincaré sphere: an appreciation, *Cur. Sci.*, **67,** 220–223.
[13] Berry, M. V., and O'Dell, D. H. J., 1998, Diffraction by volume gratings with imaginary potentials, *J. Phys.* A, **33,** 2093–2101.
[14] Berry, M. V., 1998, Lop-sided diffraction by absorbing crystals, *J. Phys.* A., **31,** 3493–3502.
[15] Karman, G. P., McDonald, G. S., Woerdman, J. P., and New, G. H. C., 1999, Excess-noise dependence on intracavity aperture shape, *Appl. Optics*, **38,** 6874–6878.
[16] McDonald, G. S., New, G. H. C., and Woerdman, J. P., 1999, Excess–noise in low Fresnel number unstable resonators, *Opt. Commun.*, **164,** 285–295.

[17] Born, M., and Wolf, E., 1959, *Principles of Optics* (London: Pergamon).
[18] Bender, C. M., and Orszag, S. A.,1978, *Advanced Mathematical Methods for Scientists and Engineers* (New York: McGraw-Hill).
[19] Wong, R., 1989, *Asymptotic Approximations to Integrals* (New York: Academic Press).